Chemical Engineering Journal 384 (2020) 123266

Contents lists available at ScienceDirect

Chemical Engineering Journal

journal homepage: www.elsevier.com/locate/cej

# Facile synthesis of nitrogen-doped reduced graphene oxide/nickel-zinc ferrite composites as high-performance microwave absorbers in the X-band

Ruiwen Shu[a,b,*], Jiabin Zhang[a], Changlian Guo[a], Yue Wu[a], Zongli Wan[a], Jianjun Shi[a], Yin Liu[c], Mingdong Zheng[a,*]

[a] School of Chemical Engineering, Anhui University of Science and Technology, Huainan 232001, People's Republic of China
[b] School of Earth and Environment, Anhui University of Science and Technology, Huainan 232001, People's Republic of China
[c] School of Materials Science and Engineering, Anhui University of Science and Technology, Huainan 232001, People's Republic of China

## HIGHLIGHTS

- NRGO/$Ni_{0.5}Zn_{0.5}Fe_2O_4$ composite was fabricated by a facile two-step strategy.
- Well-designed entanglement structure was clearly observed in the binary composite.
- Complexing of NRGO notably enhanced the microwave absorption of $Ni_{0.5}Zn_{0.5}Fe_2O_4$.
- The relationship between filler loading and refection loss was carefully clarified.
- Strong absorption, broad bandwidth and thin thickness were simultaneously achieved.

## GRAPHICAL ABSTRACT

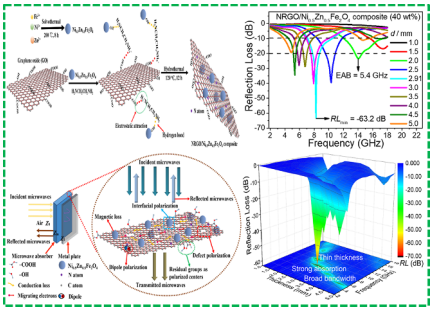


## ARTICLE INFO

*Keywords:*
Reduced graphene oxide
Nitrogen doping
Nickel-zinc ferrite
Composites
Microwave absorption

## ABSTRACT

Nowadays, developing high-performance microwave absorbers with thin thickness, strong absorbing, broad bandwidth and low filler loading is of great importance for solving the problem of electromagnetic pollution. Herein, nitrogen-doped reduced graphene oxide/nickel-zinc ferrite (NRGO/$Ni_{0.5}Zn_{0.5}Fe_2O_4$) composite was synthesized using graphene oxide (GO) as a template by a facile two-step strategy. Results of morphology observations revealed that well-designed entanglement structure consisting of $Ni_{0.5}Zn_{0.5}Fe_2O_4$ microspheres and crumpled NRGO was clearly observed in the as-prepared NRGO/$Ni_{0.5}Zn_{0.5}Fe_2O_4$ composite. Moreover, the effects of complexing of NRGO and filler loadings on the microwave absorption properties of NRGO/$Ni_{0.5}Zn_{0.5}Fe_2O_4$ composite were carefully investigated. It was found that the complexing of NRGO notably enhanced the microwave absorption properties of $Ni_{0.5}Zn_{0.5}Fe_2O_4$ microspheres. Significantly, the obtained NRGO/$Ni_{0.5}Zn_{0.5}Fe_2O_4$ composite demonstrated the optimal minimum reflection loss of −63.2 dB with a matching thickness of 2.91 mm in the X-band and effective absorption bandwidth of 5.4 GHz (12.0–17.4 GHz) almost covering the whole Ku-band with a thin thickness of merely 2.0 mm. Furthermore, the relationship between filler loading and refection loss was carefully clarified. Besides, the underlying microwave absorption mechanisms of as-prepared composite were proposed. It was believed that our results could shed light on the design and fabrication of graphene-based magnetic composites as high-efficient microwave absorbers.

* Corresponding authors at: School of Chemical Engineering, Anhui University of Science and Technology, Huainan 232001, People's Republic of China (R. Shu).
*E-mail addresses:* austshuruiwen@126.com (R. Shu), mdzheng@aust.edu.cn (M. Zheng).

https://doi.org/10.1016/j.cej.2019.123266
Received 8 July 2019; Received in revised form 16 October 2019; Accepted 21 October 2019
Available online 23 October 2019
1385-8947/ 

## 1. Introduction

With the increasingly serious problem of electromagnetic pollution originated from the extensive use of electronic equipment and devices, microwave absorbing materials (MAMs) have drawn considerable interests in the field of electromagnetic absorption [1–3]. In the past few decades, tremendous efforts have been devoted to constructing high-efficient MAMs with facile synthesis, strong microwave absorption intensity, and wide absorption bandwidth [4–11].

As a novel kind of carbon nanomaterials, reduced graphene oxide (RGO) has been considered as a potential candidate for microwave absorption due to these advantages such as low density, high specific surface areas, residual defects and oxygen-containing groups, and notable dielectric loss [12–18]. However, single RGO used as MAMs suffers from inferior impedance matching and poor attenuation loss, which greatly restrict its practical applications [12–15]. Thus, it is very urgent to enhance the microwave absorption performance of RGO for dealing with the growing problem of electromagnetic pollution.

According to the electromagnetic theories, both impedance matching and attenuation loss conditions should be well satisfied for achieving superior microwave absorption properties [4,6]. Recently, numerous investigations demonstrated that the complexation of magnetic spinel ferrites with RGO to fabricate RGO-based magnetic composites could be an effective strategy for improving the microwave absorption performance of RGO [19–37]. For instance, Wang et al. prepared the flower-like $CoFe_2O_4$@graphene composites and further investigated the microwave absorption properties of $CoFe_2O_4$@graphene/paraffin wax composites. It was observed that the obtained composites displayed the minimum reflection loss ($RL_{min}$) of −42.0 dB, and effective absorption bandwidth (EAB, $RL$ less than −10 dB) of 4.59 GHz with a thickness of 2.0 mm and filler loading of 45 wt% [30]. Yin et al. fabricated the $Ni_{0.5}Co_{0.5}Fe_2O_4$@graphene composites via one-step hydrothermal method and found that the as-prepared composites showed the $RL_{min}$ of −30.92 dB with a thickness of 4.0 mm and filler loading of 50 wt% [31]. Shen et al. synthesized the $Co_{0.8}Fe_{2.2}O_4$/RGO nanocomposites by a facile one-pot microwave hydrothermal route and observed that the as-prepared nanocomposites showed the $RL_{min}$ of −51.2 dB with a thickness of 2.1 mm, and EAB of 7.2 GHz with a thickness of 2.0 mm and filler loading of 50 wt% [35]. In our previous works, we have fabricated the RGO/$ZnFe_2O_4$ and RGO/$MnFe_2O_4$ composites by facile solvothermal and hydrothermal routes, respectively [32,33]. It was found that these two composites exhibited strong microwave absorption with thin thicknesses at very high filler loadings of 75 wt% and 70 wt%, respectively [32,33].

However, most of the reported RGO/spinel ferrites composites used as MAMs suffer from the drawbacks of unsatisfactory microwave absorption intensity ($RL_{min}$ > -60 dB), narrow absorption bandwidth (EAB < 5.0 GHz) and high filler loading ($\phi_w$ > 50 wt%). Furthermore, the relationship between structure and microwave absorption properties, and underlying microwave absorption mechanisms of RGO/spinel ferrites composites have not been clearly clarified. Therefore, it is valuable for fabricating the high-performance RGO/spinel ferrites composites and clarifying their underlying microwave absorption mechanisms. Besides, recent investigations manifested that the filler loading could significantly influence the electromagnetic parameters ($\varepsilon'$, $\varepsilon''$, $\mu'$, $\mu''$) and microwave absorption properties of MAMs according to the percolation theory [24,38–40]. Thus, it is strongly necessary for clarifying the relationship between filler loading and refection loss.

Recently, doping of RGO with heteroatoms has been regarded as an effective approach to tailor the electrical and chemical properties of RGO [2,4,41–47]. Especially, nitrogen doping in the crystal lattice of RGO could not only enhance the defects or dipole polarization and conduction loss capacity, but also optimize the impedance matching condition [2,4,41–47]. As a result, enhanced microwave absorption performance had been achieved in nitrogen-doped RGO (NRGO) and NRGO-based composites [2,4,41–47]. Combined the merits of NRGO with spinel ferrites, it is believed that superior microwave absorption properties could be achieved through fabricating the NRGO/spinel ferrites composites. To the best of our knowledge, the investigations of facile synthesis, nitrogen doping, and filler loadings on the electromagnetic parameters and microwave absorption properties of nitrogen-doped reduced graphene oxide/nickel-zinc ferrite (NRGO/$Ni_{0.5}Zn_{0.5}Fe_2O_4$) composite have been rarely reported.

Herein, we fabricated the NRGO/$Ni_{0.5}Zn_{0.5}Fe_2O_4$ composite by a facile two-step strategy. Firstly, $Ni_{0.5}Zn_{0.5}Fe_2O_4$ microspheres were synthesized through a solvothermal method; then, NRGO/$Ni_{0.5}Zn_{0.5}Fe_2O_4$ composite was prepared by a hydrothermal route. Various technique was adopted to explore the relationship between structure and microwave absorption properties of NRGO/$Ni_{0.5}Zn_{0.5}Fe_2O_4$ composite. Moreover, the influence of complexing of NRGO and filler loadings on the microwave absorption properties of NRGO/$Ni_{0.5}Zn_{0.5}Fe_2O_4$ composite was systematically investigated. Results demonstrated that the as-prepared binary composite showed comprehensively superior microwave absorption properties with strong absorption, broad bandwidth, thin thickness and low filler loading. Besides, the underlying microwave absorption mechanisms of obtained composite were clarified.

## 2. Experimental

### 2.1. Materials

Graphite oxide was provided by Suzhou TANFENG Graphene Tech Co., Ltd (Suzhou, China). Zinc chloride ($ZnCl_2$), nickel chloride ($NiCl_2{\cdot}6H_2O$), ferric chloride ($FeCl_3{\cdot}6H_2O$), sodium acetate (NaAc), ethylenediamine (EDA), ethylene glycol (EG), polyethylene glycol (PEG, $M_w$ = 6000 g·mol$^{-1}$) and anhydrous ethanol ($C_2H_5OH$) were purchased from Sinopharm Chemical Reagent Co., Ltd (Shanghai, China). All the chemical reagents were analytical grade and used without further purification. Deionized water was produced in the laboratory (electrical resistivity ~ 18.2 MΩ·cm).

### 2.2. Synthesis of $Ni_{0.5}Zn_{0.5}Fe_2O_4$ microspheres

$Ni_{0.5}Zn_{0.5}Fe_2O_4$ microspheres were synthesized by a facile solvothermal method. Firstly, 0.5 mmol of $ZnCl_2$, 0.5 mmol of $NiCl_2{\cdot}6H_2O$ and 2 mmol of $FeCl_3{\cdot}6H_2O$ were completely dissolved into 30 mL of EG by vigorous stirring. Then, 2.7 g of NaAc and 0.75 g PEG were fully dissolved into the mixture solution under vigorous stirring, respectively. Next, the homogeneous solution was poured into a Teflon-lined stainless-steel autoclave (50 mL) and reacted at 200 °C for 8 h. Afterward, the obtained product was collected by magnetic separation, and then purified by repeated washing with deionized water and anhydrous ethanol for several times. Finally, the powder-like sample was obtained by grinding dried solid product, which was dried at 55 °C for 24 h in a vacuum oven.

### 2.3. Preparation of NRGO/$Ni_{0.5}Zn_{0.5}Fe_2O_4$ composite

NRGO/$Ni_{0.5}Zn_{0.5}Fe_2O_4$ composite was fabricated using graphene oxide (GO) as a template through a hydrothermal route. Typically, aqueous GO dispersion (0.5 mg/mL) was firstly obtained by ultrasonic dispersion of graphite oxide (15 mg) into deionized water (30 mL) for 15 min and vigorous stirring for 30 min, respectively. Then, 50 mg of $Ni_{0.5}Zn_{0.5}Fe_2O_4$ powder was completely dispersed into aqueous GO dispersion by ultrasonication for 10 min and vigorous stirring for 15 min, respectively. Next, 100 μL EDA was injected into the mixture dispersion and vigorously stirred for 15 min. Afterward, the reaction mixture was poured into a Teflon-lined stainless-steel autoclave (50 mL) and reacted at 120 °C for 12 h. Finally, the resulting product was collected by magnetic separation, and then purified by repeated washing

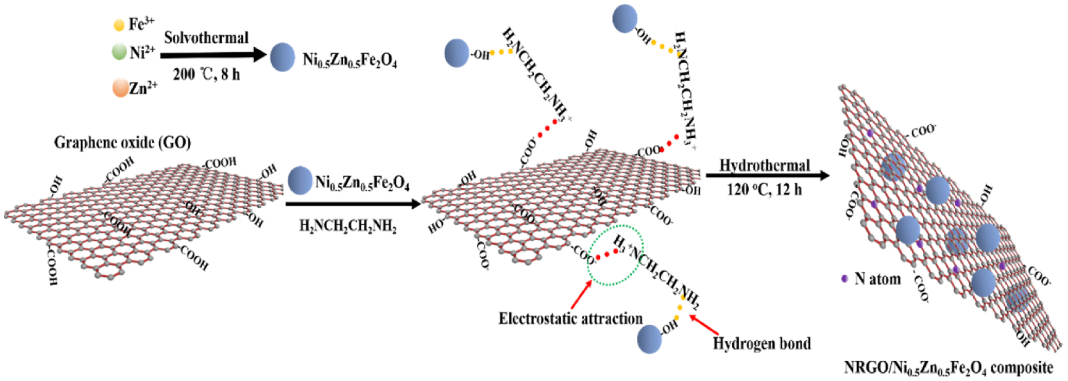


**Fig. 1.** Schematic illustration of the synthesis process of NRGO/$Ni_{0.5}Zn_{0.5}Fe_2O_4$ composite.

with deionized water and anhydrous ethanol for several times, and dried at 55 °C for 24 h in a vacuum oven. For simplicity, the as-prepared $Ni_{0.5}Zn_{0.5}Fe_2O_4$ and NRGO/$Ni_{0.5}Zn_{0.5}Fe_2O_4$ composite were labeled as S1 and S2, respectively.

The schematic synthesis procedures of NRGO/$Ni_{0.5}Zn_{0.5}Fe_2O_4$ composite were described in Fig. 1. Firstly, $Ni_{0.5}Zn_{0.5}Fe_2O_4$ microspheres were synthesized by a solvothermal route. It should be noted that the EDA in this work not only acted as the nitrogen doping reagent, but also played the role of reducing agent and strong alkali [2,47]. Then, EDA could build the chemical connections with GO and inorganic $Ni_{0.5}Zn_{0.5}Fe_2O_4$ microspheres in aqueous GO dispersion. Specifically, EDA could not only connect with negatively charged $–COO^-$ on the surfaces of GO by electrostatic attraction interactions under alkaline conditions, but also link with –OH on the surfaces of $Ni_{0.5}Zn_{0.5}Fe_2O_4$ microspheres through hydrogen bonds. Finally, $Ni_{0.5}Zn_{0.5}Fe_2O_4$ microspheres were in situ deposited on the surfaces of RGO and nitrogen atoms were doped into RGO during the hydrothermal process, and thus the NRGO/$Ni_{0.5}Zn_{0.5}Fe_2O_4$ composite was formed.

The detailed characterization sections of NRGO/$Ni_{0.5}Zn_{0.5}Fe_2O_4$ composite can be found in the Electronic Supplementary Materials.

## 3. Results and discussion

### 3.1. Structural analysis

As depicted in Fig. 2(a), the diffraction peaks from X-ray diffraction (XRD) patterns of the samples of S1 and S2 appearing at $2\theta$ = 30.2, 35.6, 43.2, 57.2 and 62.6° are in good accordance with the (2 2 0), (3 1 1), (4 0 0), (5 1 1) and (4 4 0) crystal planes of $Ni_{0.5}Zn_{0.5}Fe_2O_4$ (JCPDS 52-0278), respectively [23]. However, it is difficult to distinguish the diffraction peaks of RGO in the pattern of S2, which could be explained by the relatively low diffraction strength of RGO compared with that of $Ni_{0.5}Zn_{0.5}Fe_2O_4$ in the binary composite [47].

Degree of graphitization of obtained samples could be evaluated by Raman spectroscopy. From Fig. 2(b), both S2 and GO exhibit two obvious scattering peaks located at 1590 $cm^{-1}$ (G band) and 1347 $cm^{-1}$ (D band). The D and G bands signify the $sp^3$ defects or disorder, and $sp^2$ hybridization, respectively [6,47–49]. Generally, $I_D/I_G$ is often used to reflect the degree of disorder [6,47–49]. It can be seen that the values of $I_D/I_G$ for S2 and GO are 1.20 and 0.89, respectively. Thus, the as-prepared binary composite shows obviously enhanced $I_D/I_G$ compared with that of GO, which suggests the degree of defects become higher. This result could be originated form the introduction of numerous defects on the surfaces of RGO by nitrogen doping during the hydrothermal process [47]. Furthermore, it is obvious that the Raman scattering peaks in the low wavenumbers range (300–800 $cm^{-1}$, marked by the blue dashed box) of the samples of S1 and S2 could be ascribed to the characteristic peaks of $Ni_{0.5}Zn_{0.5}Fe_2O_4$ [50].

Thermal gravimetric analysis (TGA) measurements were conducted for determining the content of NRGO in the sample of S2. As shown in Fig. S1, the thermal decomposition behavior could be divided into two stages. Firstly, a small weight loss (~5.1 wt%) below 250 °C mainly comes from the loss of adsorbed water [36]. Secondly, an obvious weight loss from 250 °C to 550 °C, which could be ascribed to the

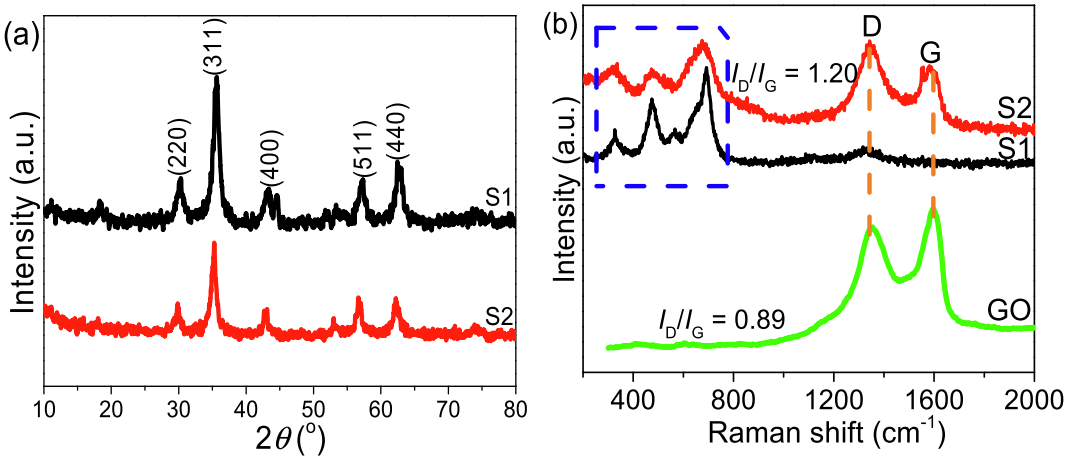


**Fig. 2.** (a) XRD patterns of the samples of S1 and S2 and (b) Raman spectra of the samples of S1, S2 and GO.

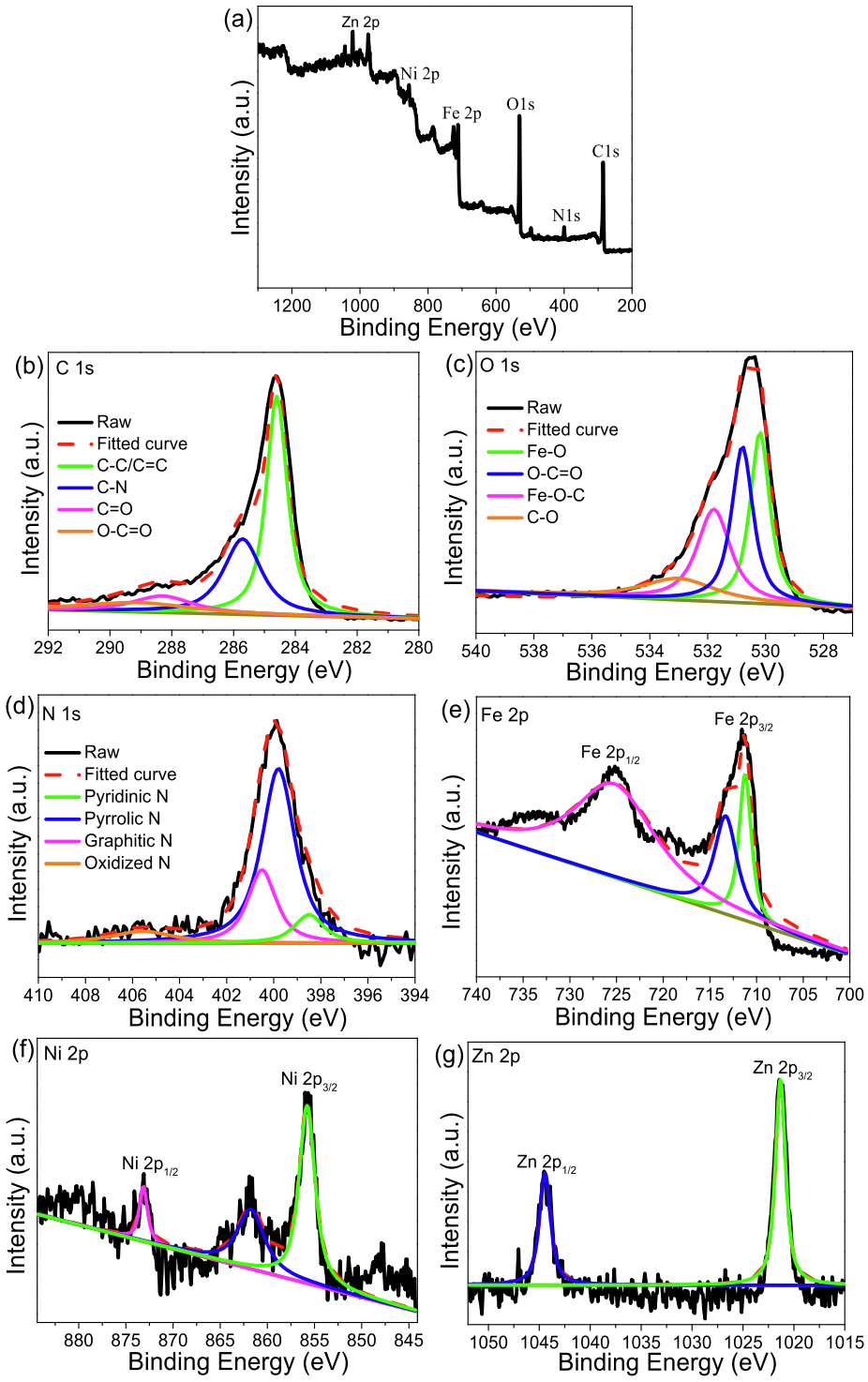


**Fig. 3.** XPS spectra of (a) wide scan, (b) C 1s, (c) O 1s, (d) N 1s, (e) Fe 2p, (f) Ni 2p and (g) Zn 2p for the sample of S2.

degradation of NRGO. Besides, the residual products are deduced to the constituent of $Ni_{0.5}Zn_{0.5}Fe_2O_4$. Thus, the content of NRGO in S2 is estimated as 23.8 wt%.

The surface chemical compositions and valence states of S2 were investigated by X-ray photoelectron spectroscopy (XPS) analysis. Fig. 3(a) shows the typical spectrum of wide scan, which confirms that the S2 contains the elements of Zn, Ni, Fe, O, N and C. As shown in Fig. 3(b), the peaks of C 1s at 289.5, 288.4, 285.6 and 284.6 eV can be assigned to O–C=O, C=O, C–N and C–C/C=C bonds, respectively [6,23,48]. From Fig. 3(c), the O 1s spectra can be fitted into four peaks of Fe–O–C, O–C=O, C–O and Fe–O [6,23,48]. As depicted in Fig. 3(d), the N 1s spectra can be split into four kinds of N (graphitic N, pyridinic N, pyrrolic N and oxidized N) [2,4,6], which suggests that the N atoms have been doped into RGO. From Fig. 3(e), the peaks at 711.3 and 713.4 eV could be assigned to Fe $2p_{3/2}$. However, the peak at 725.6 eV could be ascribed to Fe $2p_{1/2}$ [23,48]. As displayed in Fig. 3(f), the

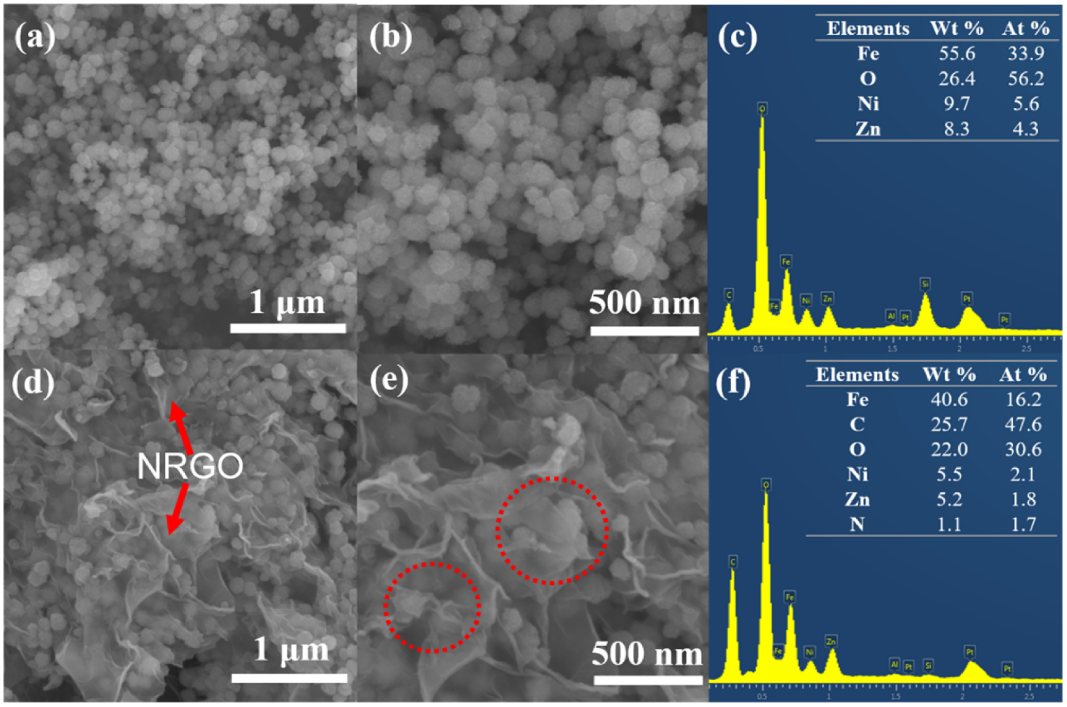


**Fig. 4.** SEM images with different magnifications: (a) and (b) S1, (d) and (e) S2; EDS patterns and elements contents: (c) S1 and (f) S2.

peaks at 855.8 and 873.2 eV could be assigned to Ni $2p_{3/2}$ and Ni $2p_{1/2}$, respectively [4,23]. From Fig. 3(g), the peaks at 1021.3 and 1044.5 eV could be ascribed to Zn $2p_{3/2}$ and Zn $2p_{1/2}$, respectively [23,48].

### 3.2. Morphological analysis

Scanning electron microscopy (SEM) was used to observe the micromorphology of the samples of S1 and S2, as shown in Fig. 4. From Fig. 4(a) and (b), it is obvious that the $Ni_{0.5}Zn_{0.5}Fe_2O_4$ particles in the S1 exhibit a spherical-like morphology. Furthermore, all the $Ni_{0.5}Zn_{0.5}Fe_2O_4$ microspheres present coarse surfaces, which derive from the self-assembly process of small primary nanocrystals in-situ formed under the solvothermal reaction conditions. Similar results have been also observed in our previous works [48,49]. As displayed in Fig. 4(d) and (e), the flake-like NRGO in the S2 shows a rippled and crumpled morphology. Furthermore, numerously micro-sized $Ni_{0.5}Zn_{0.5}Fe_2O_4$ particles with rough surfaces are uniformly loaded on the surfaces of NRGO. Remarkably, well-designed entanglement structure consisting of $Ni_{0.5}Zn_{0.5}Fe_2O_4$ microspheres and crumpled NRGO is clearly observed in the S2 (marked by the red dotted circles in Fig. 4(e)). Therefore, it is believed that abundantly heterogeneous interfaces between $Ni_{0.5}Zn_{0.5}Fe_2O_4$ microspheres and NRGO could be formed, which notably enhance the interfacial polarization and dielectric loss of S2 under the alternating electromagnetic fields. As shown in Fig. 4(c) and (f), the EDS patterns of S1 and S2 reveal that the existence of Ni, Zn, Fe and O elements. Furthermore, a little amount of N elements (1.1 wt%) have been detected in the S2, which suggests the N atoms have been doped into RGO. This finding is in good accordance with the result of XPS analysis in Fig. 3(d).

As shown in Fig. S2, the $Ni_{0.5}Zn_{0.5}Fe_2O_4$ microspheres presented statistical average size of 106.71 and 135.19 nm for the samples of S1 and S2, respectively.

The micromorphology and structure of the samples of S1 and S2 were further characterized by transmission electron microscopy (TEM), as displayed in Fig. 5. From Fig. 5(a), (b), (d) and (e), it can be observed that the $Ni_{0.5}Zn_{0.5}Fe_2O_4$ particles in both S1 and S2 exhibit spherical-like morphology. Moreover, the $Ni_{0.5}Zn_{0.5}Fe_2O_4$ microspheres in the S1 exhibit a slight aggregation, while the dispersion of $Ni_{0.5}Zn_{0.5}Fe_2O_4$ in the S2 is obviously improved and $Ni_{0.5}Zn_{0.5}Fe_2O_4$ microspheres are uniformly loaded on the surfaces of NRGO. Furthermore, the thinly flake-like NRGO in the S2 is almost transparent, which suggests few-layer structure [22,49,51]. It should be noted that almost none of $Ni_{0.5}Zn_{0.5}Fe_2O_4$ microspheres are dropped off from the surfaces of NRGO under powerful ultrasound treatment. Therefore, it is believed that the $Ni_{0.5}Zn_{0.5}Fe_2O_4$ microspheres are tightly anchored on the surfaces of NRGO [49,51]. As shown in the high-resolution transmission electron microscopy (HRTEM) images of Fig. 5(c) and (f), the interplane distances of 0.305 and 0.245 nm correspond to the (2 2 0) and (3 1 1) crystal planes of $Ni_{0.5}Zn_{0.5}Fe_2O_4$, respectively.

Fig. S3 shows the EDS element mappings images, which illustrate the existence of C, Zn, Ni, Fe and O with an almost homogeneous elemental distribution in the sample of S2.

### 3.3. Magnetic properties

The magnetic hysteresis loops of the samples of S1 and S2 were acquired by a vibrating sample magnetometer (VSM) at room temperature. As shown in the inset of Fig. 6, the magnified magnetization curves clearly demonstrate that both S1 and S2 display typically ferromagnetic behaviors, which could generate notable magnetic loss in the gigahertz frequency region [52,53]. Specifically, the saturation magnetization ($M_s$) of S1 and S2 is 64.8 and 57.7 emu/g, respectively. It should be noted that the ferromagnetism of S1 and S2 mainly originates from the $Ni_{0.5}Zn_{0.5}Fe_2O_4$ microspheres. Therefore, the S2 presents a notable decrease of $M_s$ compared with S1, which could be ascribed to the introduction of non-magnetic RGO in the binary composite [49].

### 3.4. Microwave absorption properties

This work focused on exploring the influence of filler loadings on the electromagnetic parameters and microwave absorption properties of NRGO/$Ni_{0.5}Zn_{0.5}Fe_2O_4$ composite. From Fig. 7(a)–(d), the values of

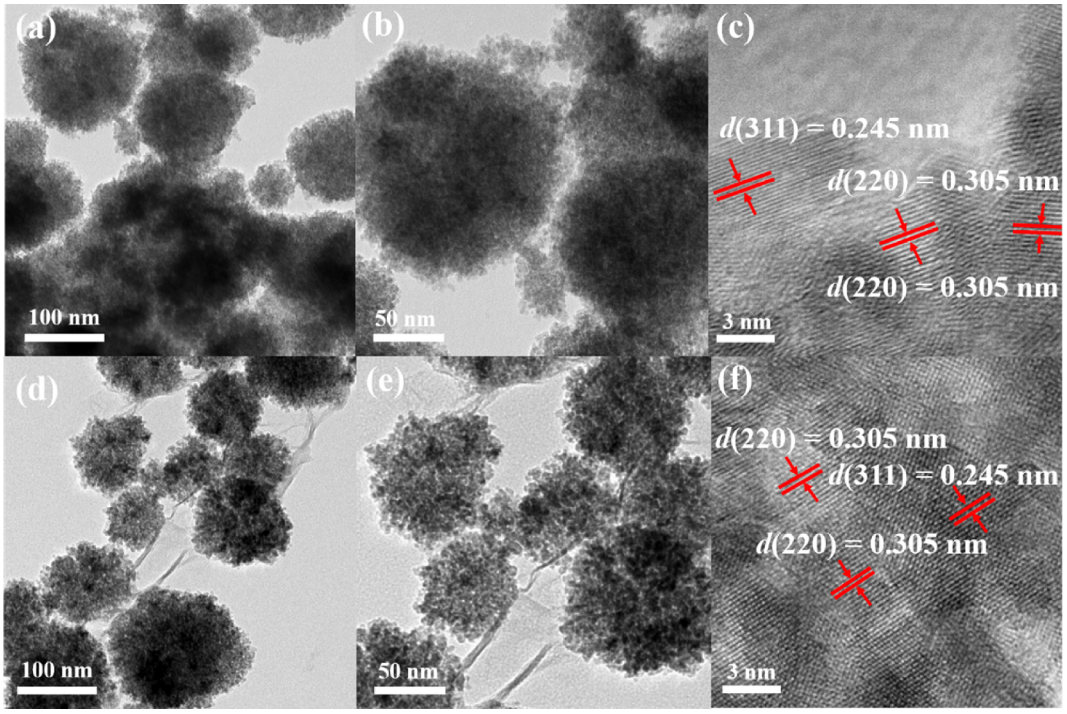


**Fig. 5.** TEM images with different magnifications: (a) and (b) S1, (d) and (e) S2; HRTEM images: (c) S1 and (f) S2.

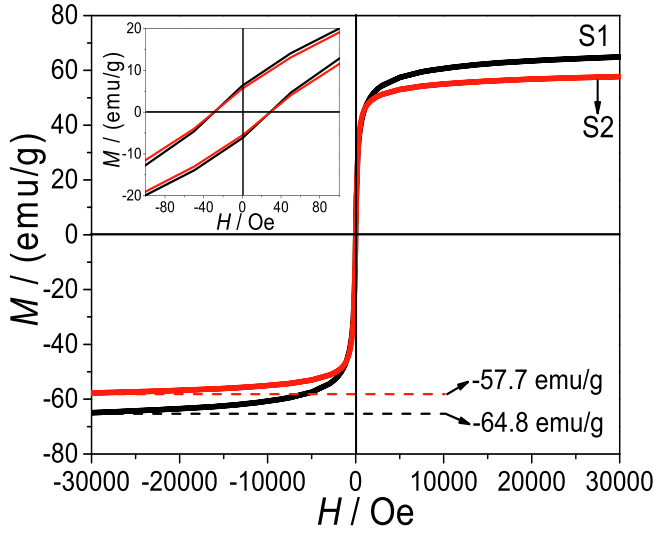


**Fig. 6.** Magnetic hysteresis loops of the samples of S1 and S2 at room temperature. Inset: the magnified magnetization curves at the low field.

$RL_{min}$ of S2 achieve −10.8, −17.8, −63.2, −17.8 and −10.8 dB as the filler loadings are 30, 35, 40, 50 and 60 wt%, respectively. Notably, the S2 presents a broad EAB of 5.4 GHz (12.0–17.4 GHz) for a thickness of merely 2.0 mm and filler loading of 40 wt%. It can be concluded that the S2 exhibits the optimal microwave absorption performance at a filler loading of 40 wt%. As described in Fig. 7(e), the S1 shows the $RL_{min}$ of merely −6.7 dB, which suggests the poor microwave absorption performance. Therefore, the S2 (NRGO/$Ni_{0.5}Zn_{0.5}Fe_2O_4$ composite) demonstrated obviously enhanced microwave absorption performance compared with S1 (pure $Ni_{0.5}Zn_{0.5}Fe_2O_4$). To intuitively evaluate the variation trend of $RL_{min}$ with $\phi_w$, the $|RL_{min}| \sim \phi_w$ curve was plotted for the S2, as depicted in Fig. 7(g). It can be found that the $|RL_{min}|$ firstly increases and then decreases with the increasing of filler loadings. Remarkably, the S2 exhibits the best microwave absorption properties with the filler loading of 40 wt%. Fig. 7(h) and (i) display the three-dimensional (3D) plots of reflection loss for S1 and S2. Remarkably, the $RL_{min}$ corresponding to the maximum microwave absorption could locate at various frequencies by modulating the thicknesses of absorbers [6,48].

Generally, the electromagnetic parameters ($\varepsilon'$, $\varepsilon''$, $\mu'$, $\mu''$) are vitally important to determine the microwave absorption properties [6,48,49]. The real permittivity ($\varepsilon'$) and real permeability ($\mu'$) represent the storage ability of electric and magnetic field energy, whereas the imaginary permittivity ($\varepsilon''$) and imaginary permeability ($\mu''$) indicate the dissipation capacity of electric and magnetic field energy, respectively [6,48,49]. Thus, the frequency dependence of electromagnetic parameters of S2 with different filler loadings was carefully investigated, as depicted in Fig. 8(a)–(d). From Fig. 8(a), the $\varepsilon'$ of S2 at all filler loadings shows a decline trend with the increasing of frequency and reveals a frequency dispersion effect, which is beneficial to the microwave absorption [54]. Specifically, the $\varepsilon'$ decreases from 6.3 to 4.8, 9.0 to 6.9, 11.9 to 8.2, 16.2 to 8.1, 21.8 to 9.8 for the filler loadings of 30 wt%, 35 wt%, 40 wt%, 50 wt% and 60 wt%, respectively. Therefore, the $\varepsilon'$ enhances as the filler loadings increase. As shown in Fig. 8(b), the $\varepsilon''$ of S2 for the filler loading larger than 40 wt% decreases with the increasing of frequency. Similarly, the $\varepsilon''$ also enhances with the increasing of filler loadings. On the basis of free electron theory, it can be deduced that the $\varepsilon''$ enhances with the increasing of electrical conductivity [6,55,56]. In the present study, the specimens for the measurements of electromagnetic parameters were prepared by uniformly mixing the as-prepared NRGO/$Ni_{0.5}Zn_{0.5}Fe_2O_4$ composite into the paraffin matrix at different filler loadings. We have measured the electrical conductivity of obtained $Ni_{0.5}Zn_{0.5}Fe_2O_4$ microspheres, NRGO/$Ni_{0.5}Zn_{0.5}Fe_2O_4$ composite and paraffin wax by a four-point probe method. The measured values of electrical conductivity for $Ni_{0.5}Zn_{0.5}Fe_2O_4$ microspheres, NRGO/$Ni_{0.5}Zn_{0.5}Fe_2O_4$ composite and paraffin wax are $6 \times 10^{-6}$, 15.4 and $5 \times 10^{-8}$ S/m, respectively. Therefore, the S2 (NRGO/$Ni_{0.5}Zn_{0.5}Fe_2O_4$ composite) demonstrates

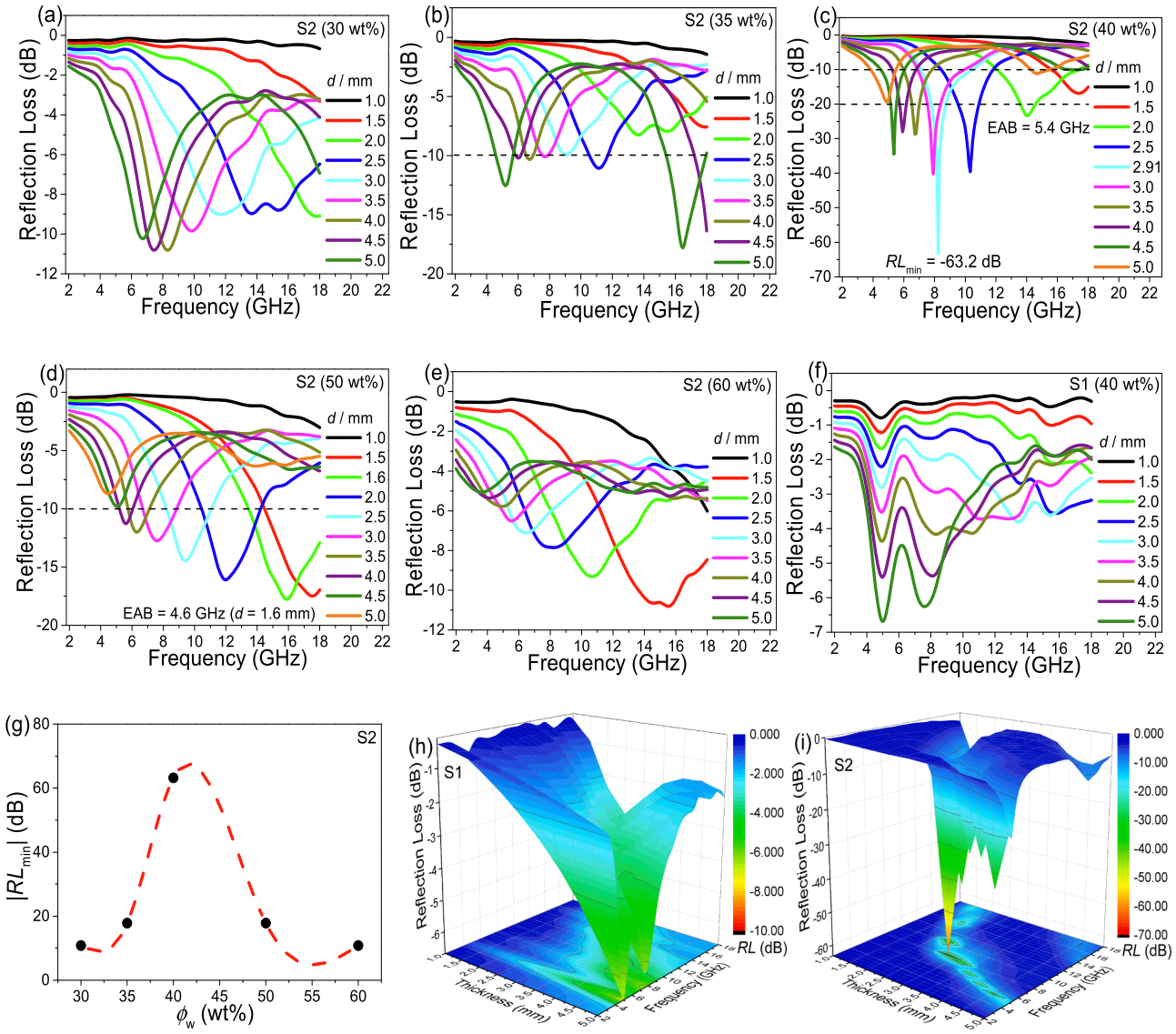


**Fig. 7.** Frequency dependence of reflection loss at different thicknesses for the sample of S2 with various filler loadings: (a) 30 wt%, (b) 35 wt%, (c) 40 wt%, (d) 50 wt % and (e) 60 wt%; Frequency dependence of reflection loss at different thicknesses for S1 with a filler loading of 40 wt% (f); Absolute value of $RL_{min}$ as a function of filler loadings for the sample of S2 (g); 3D representations of reflection loss for S1 (h) and S2 (i) with a filler loading of 40 wt%, respectively.

obviously enhanced electrical conductivity than that of S1 (pure $Ni_{0.5}Zn_{0.5}Fe_2O_4$). It could be deduced that the electrical conductivity of NRGO/$Ni_{0.5}Zn_{0.5}Fe_2O_4$/paraffin wax composites increases with the increasing of filler loadings, leading to the enhanced $\varepsilon''$. Numerous investigations demonstrated that $\varepsilon'$ kept pace with the variation in electric conductivity and there existed identical change rules about $\varepsilon'$ and $\varepsilon''$ [54,57,58]. Therefore, the S2 with the filler loading of 60 wt% exhibits the biggest $\varepsilon'$ and $\varepsilon''$, which manifests the enhanced storage capability of electric energy and dielectric loss [54,59]. From Fig. 8(c), the $\mu'$ of S2 at all filler loadings presents some fluctuations with the increasing of frequency and the values of $\mu'$ are in the range of 0.8–1.3. As described in Fig. 8(d), the $\mu''$ of S2 at all filler loadings presents a notably decreasing trend as the frequency increases in the frequency range of 2–6 GHz.

Attenuation loss includes dielectric loss and magnetic loss, which plays a vital role in microwave attenuation [6,48]. Thus, the frequency-dependent dielectric loss tangent ($\tan\delta_e = \varepsilon''/\varepsilon'$) and magnetic loss tangent ($\tan\delta_m = \mu''/\mu'$) for the sample of S2 with different filler loadings were investigated. From Fig. 8(e), the S2 exhibits obviously enhanced $\tan\delta_e$ with the increasing of filler loadings, suggesting the improved dielectric loss against the incident microwaves. It should be noted that the obviously enhanced dielectric loss could be attributed to the notably increased $\varepsilon'$ and $\varepsilon''$ of S2 as the filler loadings increasing. As depicted in Fig. 8(f), the $\tan_m$ of S2 displays a similar tendency as $\mu''$ with the increasing of frequency for all the filler loadings. Besides, combined Fig. 8(e) with Fig. 8(f), it can be found that both dielectric loss and magnetic loss play important roles for the microwave attenuation.

The eddy current loss can be evaluated by the following equations [6,48,49,52]:

$$\mu'' \approx 2\pi\mu_0(\mu')^2\sigma d^2 f/3 \quad (1)$$

$$C_0 = \mu''(\mu')^{-2}f^{-1} \quad (2)$$

Herein $C_0$ is eddy current coefficient, σ is the electric conductivity, $\mu_0$ is the vacuum permeability and $d$ is the thickness of absorber. If magnetic loss mainly originates from eddy current effect, the values of $C_0$ should keep constant as the frequency increasing [6,48,49,52]. Fig. 9 displays plots of $C_0$ vs. frequency for the sample of S2 with different filler loadings. Notably, $C_0$ decreases with the increasing of frequency, which indicates that the eddy loss is relatively weak and that magnetic

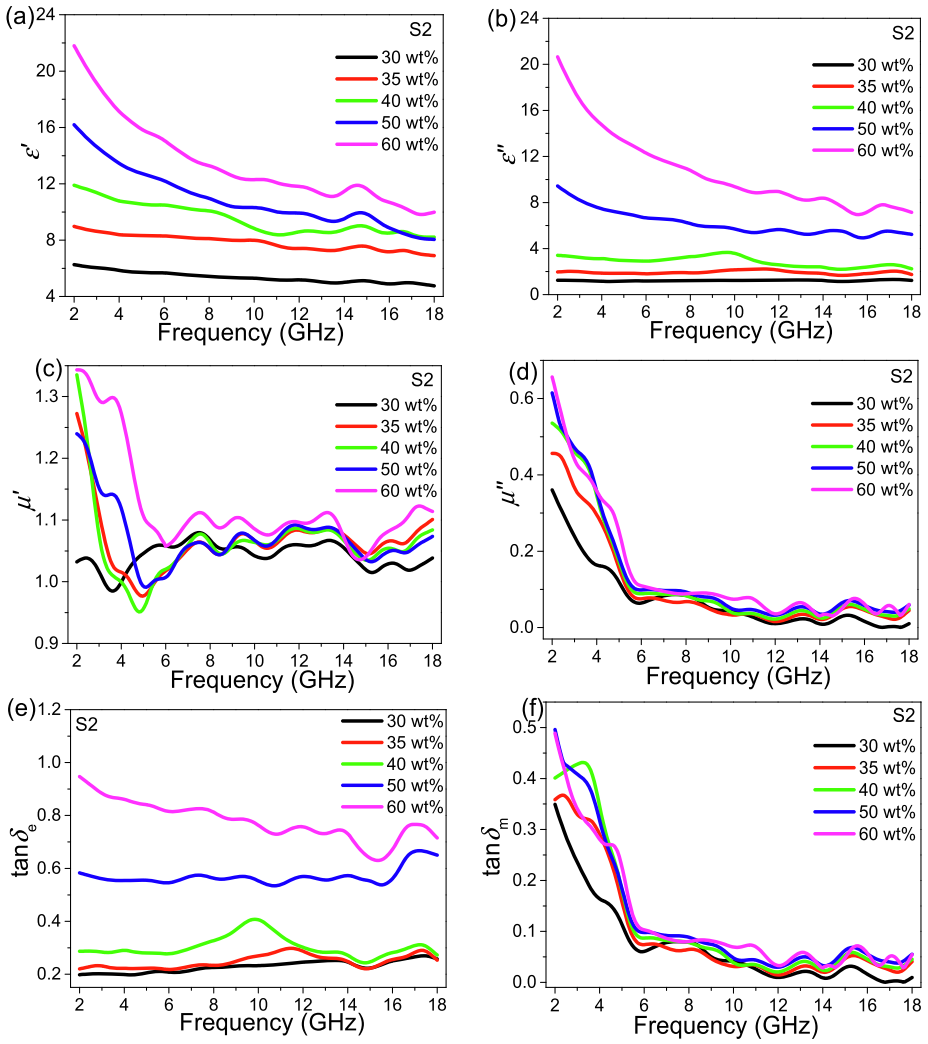


**Fig. 8.** Frequency dependence of (a) $\varepsilon'$, (b) $\varepsilon''$, (c) $\mu'$, (d) $\mu''$, (e) $\tan\delta_e$ and (f) $\tan\delta_m$ for the sample of S2 with different filler loadings.

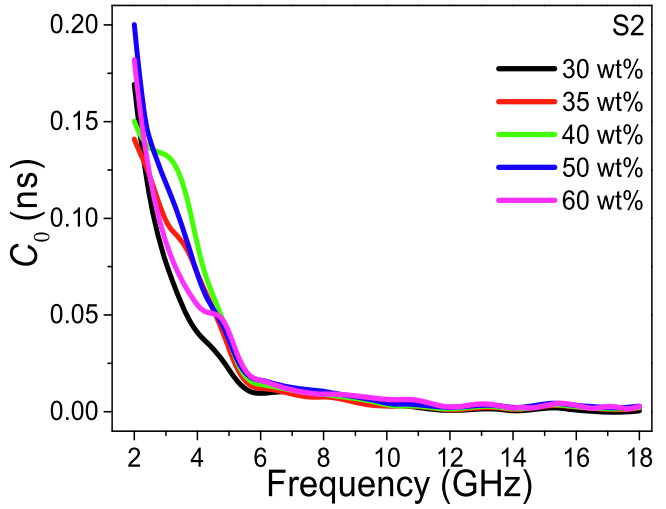


**Fig. 9.** Frequency dependence of $C_0$ for the sample of S2 with different filler loadings.

loss mainly originates from the magnetic resonance [60].

Numerous investigations demonstrated that the quarter-wavelength (1/4λ) cancellation mechanism and impedance matching could be used to explain the microwave absorption mechanisms including the origin, position and intensity of reflection loss (*RL*) peaks, respectively [60–62]. The modulus of the normalized input impedance $|Z_{in}/Z_0|$ is often described as follows [6,62–65]:

$$\left|\frac{Z_{in}}{Z_0}\right| = \left|\sqrt{\frac{\mu_r}{\varepsilon_r}}\tanh\left[j\left(\frac{2\pi fd}{c}\right)\sqrt{\mu_r\varepsilon_r}\right]\right| \quad (3)$$

Herein, $Z_0$ is the impedance of air, and $Z_{in}$ is the input impedance of the sample.

If the thickness of the absorber ($t_m$) at the absorption peak frequency ($f_m$) satisfies the equation [54,60–62]:

$$t_m = \frac{n\lambda}{4} = \frac{nc}{4f_m\sqrt{|\varepsilon_r\mu_r|}}(n = 1, 3, 5, \ldots) \quad (4)$$

where $c$ is the velocity of light in free space, $|\mu_r|$ and $|\mu_r|$ are the moduli of $\mu_r$ and $\varepsilon_r$, the incident and reflected waves in the absorbers are out of phase by 180°, resulting in the disappearance of each other at the air-absorber interface [54].

Fig. 10 shows the dependence of *RL* on frequency at 1/4λ thicknesses for the sample of S2 with a filler loading of 40 wt%, and the $|Z_{in}/Z_0|$ is calculated at the same time. The pentagram signifies the experimental $t_m$ (denoted as $t_m^{exp}$). As shown in Fig. 10, the $RL_{min}$ of −63.2 dB is found at the thickness of 2.91 mm and frequency of 8.24 GHz when the $|Z_{in}/Z_0|$ equals approximately 1. This is the perfect matching point in this circumstance [62]. Therefore, the S2 with the filler loading of 40 wt% could simultaneously satisfy the 1/4

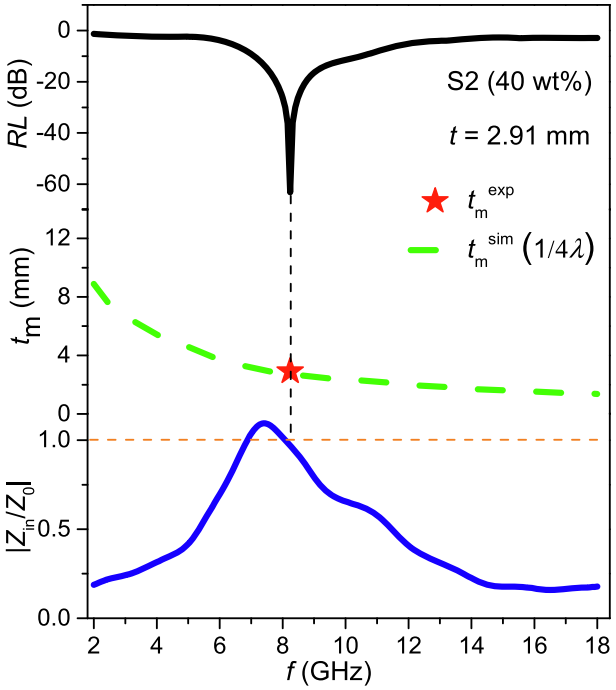


**Fig. 10.** Dependence of *RL* on frequency at 1/4λ thicknesses and the $|Z_{in}/Z_0|$ for the sample of S2 with a filler loading of 40 wt%.

wavelength formula and optimal impedance matching, which leads to the formation of minimum reflection loss.

Fig. 11 describes the possible microwave absorption mechanisms of NRGO/$Ni_{0.5}Zn_{0.5}Fe_2O_4$ composite. We assume that the microwaves are incident normally from the front of absorber (NRGO/$Ni_{0.5}Zn_{0.5}Fe_2O_4$ composite) and are backed by a perfect conductor (metal plate). The underlying microwave absorption mechanisms of NRGO/$Ni_{0.5}Zn_{0.5}Fe_2O_4$ composite could be ascribed to the following reasons. Firstly, the residual oxygen-containing groups such as –COOH and –OH, and structure defects on the surface of RGO could induce the dipole polarization and defect polarization under the alternating electromagnetic fields, respectively [49,51]. Secondly, numerously heterogeneous interfaces among paraffin matrix, NRGO and $Ni_{0.5}Zn_{0.5}Fe_2O_4$ significantly enhance the interfacial polarization relaxation [6,48,49,51]. Thirdly, nitrogen-doping in the crystal lattice of RGO, which not only enhances the dipole polarization relaxation, but also improves the conduction loss [2,4,6,42,43]. Fourthly, according to the Cao's electrons hopping model [66,67], the electrons can absorb electromagnetic energies to migrate on the surface of NRGO, and then convert the electromagnetic energies into thermal energies by colliding with the lattice [68]. Lastly, the synergistic effects of dielectric loss derived from interfacial polarization, defect polarization and dipole polarization, magnetic loss originated from ferromagnetic $Ni_{0.5}Zn_{0.5}Fe_2O_4$ microspheres, and conduction loss coming from NRGO, which significantly improve the microwave attenuation capacity and optimize the impedance matching.

For the sake of evaluating the microwave absorption properties of as-prepared NRGO/$Ni_{0.5}Zn_{0.5}Fe_2O_4$ composite in this work, we have compared our results with previously similar RGO (or graphene)-based spinel ferrites composites reported in the open literatures. As shown in Table 1, it can be found that the obtained NRGO/$Ni_{0.5}Zn_{0.5}Fe_2O_4$ composite (S2) exhibits comprehensively optimal microwave absorption performance among all the reported similar composites with the $RL_{min}$ of −63.2 dB at a thickness of 2.91 mm and a broad EAB of 5.4 GHz at a thin thickness of only 2.0 mm. Therefore, we believe that the as-prepared NRGO/$Ni_{0.5}Zn_{0.5}Fe_2O_4$ composite in this work could show great potential for practical applications as high-performance microwave absorbers in the field of electromagnetic absorption.

## 4. Conclusions

In summary, NRGO/$Ni_{0.5}Zn_{0.5}Fe_2O_4$ composite was successfully prepared by a facile two-step strategy. Results of morphology observations demonstrated that well-designed entanglement structure consisting of $Ni_{0.5}Zn_{0.5}Fe_2O_4$ microspheres and crumpled NRGO was found in the as-prepared NRGO/$Ni_{0.5}Zn_{0.5}Fe_2O_4$ composite. Moreover, the as-prepared binary composite exhibited obviously enhanced microwave absorption properties compared with single $Ni_{0.5}Zn_{0.5}Fe_2O_4$ microspheres. Furthermore, the relationship between filler loading and refection loss was well clarified by the $|RL_{min}| \sim \phi_w$ curve. Significantly, the obtained composite showed comprehensively superior microwave absorption properties with strong absorption, broad bandwidth, thin thickness and low filler loading. Besides, the underlying microwave absorption mechanisms of as-prepared composite were proposed, which could be ascribed to the enhanced polarization relaxation, synergistic effects of magnetic loss, conduction loss and dielectric loss, and optimized impedance matching. Therefore, the obtained composite in this work could be used as high-efficiency microwave absorbers in the field of electromagnetic absorption.

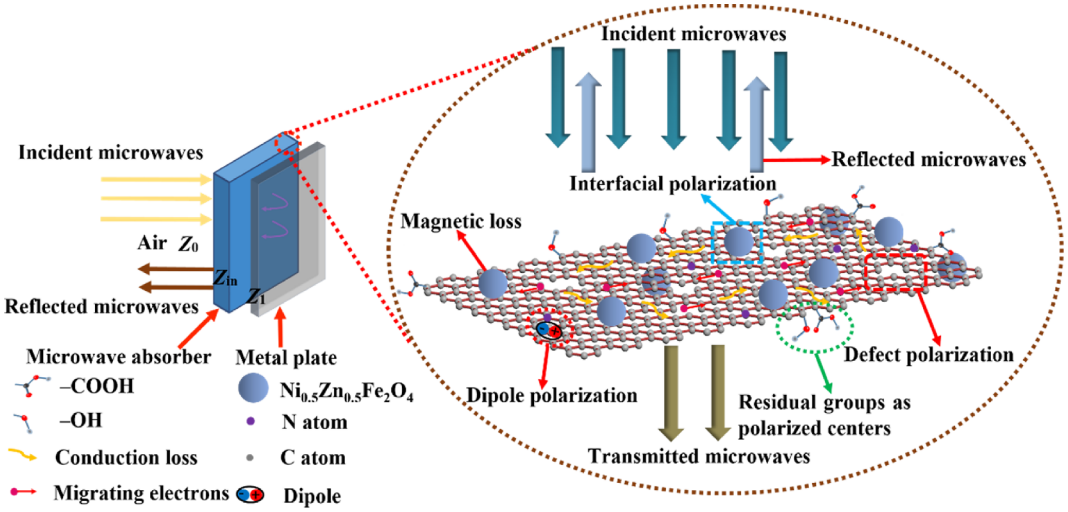


**Fig. 11.** Schematic illustration of the possible microwave absorption mechanisms of NRGO/$Ni_{0.5}Zn_{0.5}Fe_2O_4$ composite.

**Table 1**
Typical RGO (or graphene)-based spinel ferrites composites used as microwave absorbers reported in this work and recent literatures.

| Sample | Matrix | Filler loading (wt%) | $RL_{min}$ (dB) | EAB (GHz) | Thickness (mm) | Ref. |
|---|---|---|---|---|---|---|
| S2 (NRGO/$Ni_{0.5}Zn_{0.5}Fe_2O_4$) | Paraffin | 40 | −63.2 | 5.4 | 2.0 | This work |
| S2 (NRGO/$Ni_{0.5}Zn_{0.5}Fe_2O_4$) | Paraffin | 50 | −17.8 | 4.6 | 1.6 | This work |
| $NiFe_2O_4$ nanorod-graphene | Paraffin | 60 | −29.2 | 4.4 | 3.0 | [19] |
| RGO-$Fe_3O_4$ | Paraffin | 50 | −44.6 | 4.3 | 2.0 | [20] |
| $CoFe_2O_4$/graphene | Paraffin | 60 | −24.7 | 3.7 | 2.0 | [21] |
| $ZnFe_2O_4$/RGO | Paraffin | 30 | −29.3 | 2.6 | 1.6 | [22] |
| RGO-$Ni_{0.5}Zn_{0.5}Fe_2O_4$ | Paraffin | / | −47.8 | 4.8 | 2.0 | [23] |
| $NiFe_2O_4$/rGO | Paraffin | 50 | −42.0 | 5.3 | 6.5 | [24] |
| $Co_{0.2}Ni_{0.4}Zn_{0.4}Fe_2O_4$/graphene | Paraffin | 40 | −53.5 | 4.8 | 3.1 | [25] |
| RGO/$Ni_{0.5}Zn_{0.5}Co_{0.2}Fe_2O_4$ | Paraffin | 40 | −57.6 | 4.2 | 3.0 | [26] |
| $NiFe_2O_4$-rGO | Paraffin | / | −58.0 | 4.08 | 2.7 | [27] |
| $CoFe_2O_4$/RGO | Paraffin | 50 | −57.7 | 5.8 | 2.8 | [28] |
| Hollow $NiFe_2O_4$/graphene | Paraffin | 15 | −40.9 | 2.8 | 3.5 | [29] |
| $CoFe_2O_4$@graphene | Paraffin | 45 | −42.0 | 4.59 | 2.0 | [30] |
| $Ni_{0.5}Co_{0.5}Fe_2O_4$@graphene | Paraffin | 50 | −30.92 | / | 4.0 | [31] |
| RGO/$ZnFe_2O_4$ | Paraffin | 75 | −41.1 | 3.2 | 2.0 | [32] |
| RGO/$MnFe_2O_4$ | Paraffin | 70 | −47.5 | 5.2 | 1.7 | [33] |
| $Co_{0.33}Ni_{0.33}Mn_{0.33}Fe_2O_4$/graphene | Paraffin | 20 | −24.29 | 8.48 | 2.3 | [34] |
| $Co_{0.8}Fe_{2.2}O_4$/rGO | Paraffin | 50 | −51.2 | 7.2 | 2.0 | [35] |
| $CoFe_2O_4$/rGO | Paraffin | 50 | −56.8 | 6.8 | 2.2 | [36] |
| $Ni_{0.33}Co_{0.67}Fe_2O_4$@rGO | Paraffin | 20 | −47.5 | 5.02 | 2.0 | [37] |

*Notes:* RGO or rGO denoted reduced graphene oxide.

## Declaration of Competing Interest

The authors declare that they have no known competing financial interests or personal relationships that could have appeared to influence the work reported in this paper.

## Acknowledgments

This work was financially supported by the Foundation of Provincial Natural Science Research Project of Anhui Colleges (Grant Nos. KJ2019A0119, KJ2017ZD09), China Postdoctoral Science Foundation (Grant No. 2019M652160), National Natural Science Foundation of China (Grant No. 51507003), Lift Engineering of Young Talents and Doctor's Start-up Research Foundation of Anhui University of Science and Technology (Grant No. ZY537).

## Appendix A. Supplementary data

Supplementary data to this article can be found online at https://doi.org/10.1016/j.cej.2019.123266.

## References

[1] H. Lv, Z. Yang, S. Hoong Ong, C. Wei, H. Liao, S. Xi, Y. Du, G. Ji, Z. Xu, A flexible microwave shield with tunable frequency-transmission and electromagnetic compatibility, Adv. Funct. Mater. 29 (2019) 1900163.
[2] P. Liu, Y. Zhang, J. Yan, Y. Huang, L. Xia, Z. Guang, Facile synthesis of ultralightweight N-doped graphene foams with open reticular structures for high-efficiency electromagnetic wave absorption performance, Chem. Eng. J. 368 (2019) 285–298.
[3] L. Kong, X. Yin, H. Xu, X. Yuan, T. Wang, Z. Xu, J. Huang, R. Yang, H. Fan, Powerful absorbing and lightweight electromagnetic shielding CNTs/RGO composite, Carbon 145 (2019) 61–66.
[4] Y. Wang, X. Gao, X. Wu, W. Zhang, C. Luo, P. Liu, Facile design of 3D hierarchical $NiFe_2O_4$/N-GN/ZnO composite as a high performance electromagnetic wave absorber, Chem. Eng. J. 375 (2019) 121942.
[5] Z. Xiang, Y. Song, J. Xiong, Z. Pan, X. Wang, L. Liu, R. Liu, H. Yang, W. Lu, Enhanced electromagnetic wave absorption of nanoporous $Fe_3O_4$@carbon composites derived from metal-organic frameworks, Carbon 142 (2019) 20–31.
[6] R. Shu, W. Li, Y. Wu, J. Zhang, G. Zhang, Nitrogen-doped Co-C/MWCNTs nanocomposites derived from bimetallic metal-organic frameworks for electromagnetic wave absorption in the X-band, Chem. Eng. J. 362 (2019) 513–524.
[7] Y. Wang, X. Gao, Y. Fu, X. Wu, Q. Wang, W. Zhang, C. Luo, Enhanced microwave absorption performances of polyaniline/graphene aerogel by covalent bonding, Compos. Part B-Eng. 169 (2019) 221–228.
[8] Z. Lou, C. Yuan, Y. Zhang, Y. Li, J. Cai, L. Yang, W. Wang, H. Han, J. Zou, Synthesis of porous carbon matrix with inlaid $Fe_3C$/$Fe_3O_4$ micro-particles as an effective electromagnetic wave absorber from natural wood shavings, J. Alloy. Compd. 775 (2019) 800–809.
[9] L. Wang, Y. Guan, X. Qiu, H. Zhu, S. Pan, M. Yu, Q. Zhang, Efficient ferrite/Co/porous carbon microwave absorbing material based on ferrite@metal–organic framework, Chem. Eng. J. 326 (2017) 945–955.
[10] X. Qiu, L. Wang, H. Zhu, Y. Guan, Q. Zhang, Lightweight and efficient microwave absorbing materials based on walnut shell-derived nano-porous carbon, Nanoscale 9 (2017) 7408–7418.
[11] P. Liu, V. Ng, Z. Yao, J. Zhou, Y. Lei, Z. Yang, H. Lv, L. Kong, Facile synthesis and hierarchical assembly of flowerlike NiO structures with enhanced dielectric and microwave absorption properties, ACS Appl. Mater. Interfaces 9 (2017) 16404–16416.
[12] C. Wang, X. Han, P. Xu, X. Zhang, Y. Du, S. Hu, J. Wang, X. Wang, The electromagnetic property of chemically reduced graphene oxide and its application as microwave absorbing material, Appl. Phys. Lett. 98 (2011) 072906.
[13] H. Lv, Y. Guo, Z. Yang, Y. Cheng, L.P. Wang, B. Zhang, Y. Zhao, Z.J. Xu, G. Ji, A brief introduction to the fabrication and synthesis of graphene based composites for the realization of electromagnetic absorbing materials, J. Mater. Chem. C 5 (2017) 491–512.
[14] F. Meng, H. Wang, F. Huang, Y. Guo, Z. Wang, D. Hui, Z. Zhou, Graphene-based microwave absorbing composites: a review and prospective, Compos. Part B-Eng. 137 (2018) 260–277.
[15] M. Cao, C. Han, X. Wang, M. Zhang, Y. Zhang, J. Shu, H. Yang, X. Fang, J. Yuan, Graphene nanohybrids: superior electromagnetic properties for the absorbing and shielding of electromagnetic waves, J. Mater. Chem. C 6 (2018) 4586–4602.
[16] T. Zhu, W. Shen, X. Wang, Y. Song, W. Wang, Paramagnetic $CoS_2$@$MoS_2$ core-shell composites coated by reduced graphene oxide as broadband and tunable high-performance microwave absorbers, Chem. Eng. J. 378 (2019) 122159.
[17] J. Luo, L. Yue, H. Ji, K. Zhang, N. Yu, Investigation on the optimization, design and microwave absorption properties of $BaTb_{0.2}Eu_{0.2}Fe_{11.6}O_{19}$/PANI decorated on reduced graphene oxide nanocomposites, J. Mater. Sci. 54 (2019) 6332–6346.
[18] Y. Zhang, S. Gao, H. Xing, Reduced graphene oxide wrapped cube-like $ZnSnO_3$: as a high-performance microwave absorber, J. Alloy. Compd. 777 (2019) 544–553.
[19] M. Fu, Q. Jiao, Y. Zhao, Preparation of $NiFe_2O_4$ nanorod-graphene composites via an ionic liquid assisted one-step hydrothermal approach and their microwave absorbing properties, J. Mater. Chem. A 1 (2013) 5577–5586.
[20] M. Zong, Y. Huang, Y. Zhao, X. Sun, C. Qu, D. Luo, J. Zheng, Facile preparation, high microwave absorption and microwave absorbing mechanism of RGO–$Fe_3O_4$ composites, RSC Adv. 3 (2013) 23638–23648.
[21] M. Fu, Q. Jiao, Y. Zhao, H. Li, Vapor diffusion synthesis of $CoFe_2O_4$ hollow sphere/graphene composites as absorbing materials, J. Mater. Chem. A 2 (2014) 735–744.
[22] Z. Yang, Y. Wan, G. Xiong, D. Li, Q. Li, C. Ma, R. Guo, H. Luo, Facile synthesis of $ZnFe_2O_4$/reduced graphene oxide nanohybrids for enhanced microwave absorption properties, Mater. Res. Bull. 61 (2015) 292–297.
[23] M. Zong, Y. Huang, N. Zhang, Reduced graphene oxide–$Ni_{0.5}Zn_{0.5}Fe_2O_4$ composite: synthesis and electromagnetic absorption properties, Mater. Lett. 145 (2015) 115–119.
[24] J. He, X. Wang, Y. Zhang, M. Cao, Small magnetic nanoparticles decorating reduced graphene oxides to tune the electromagnetic attenuation capacity, J. Mater. Chem. C 4 (2016) 7130–7140.
[25] P. Liu, Z. Yao, J. Zhou, Z. Yang, L. Kong, Small magnetic Co-doped NiZn ferrite/graphene nanocomposites and their dual-region microwave absorption performance, J. Mater. Chem. C 4 (2016) 9738–9749.
[26] P. Liu, Z. Yao, J. Zhou, Fabrication and microwave absorption of reduced graphene

oxide/$Ni_{0.4}Zn_{0.4}Co_{0.2}Fe_2O_4$ nanocomposites, Ceram. Int. 42 (2016) 9241–9249.
[27] Y. Zhang, X. Wang, M. Cao, Confinedly implanted $NiFe_2O_4$-rGO: cluster tailoring and highly tunable electromagnetic properties for selective-frequency microwave absorption, Nano Res. 11 (2018) 1426–1436.
[28] Y. Liu, Z. Chen, Y. Zhang, R. Feng, X. Chen, C. Xiong, L. Dong, Broadband and lightweight microwave absorber constructed by in situ growth of hierarchical $CoFe_2O_4$/reduced graphene oxide porous nanocomposites, ACS Appl. Mater. Interfaces 10 (2018) 13860–13868.
[29] F. Yan, D. Guo, S. Zhang, C. Li, C. Zhu, X. Zhang, Y. Chen, An ultra-small $NiFe_2O_4$ hollow particle/graphene hybrid: fabrication and electromagnetic wave absorption property, Nanoscale 10 (2018) 2697–2703.
[30] S. Wang, Y. Zhao, H. Xue, J. Xie, C. Feng, H. Li, D. Shi, S. Muhammad, Q. Jiao, Preparation of flower-like $CoFe_2O_4$@graphene composites and their microwave absorbing properties, Mater. Lett. 223 (2018) 186–189.
[31] P. Yin, Y. Deng, L. Zhang, W. Wu, J. Wang, X. Feng, X. Sun, H. Li, Y. Tao, One-step hydrothermal synthesis and enhanced microwave absorption properties of $Ni_{0.5}Co_{0.5}Fe_2O_4$/graphene composites in low frequency band, Ceram. Int. 44 (2018) 20896–20905.
[32] R. Shu, G. Zhang, J. Zhang, X. Wang, M. Wang, Y. Gan, J. Shi, J. He, Synthesis and high-performance microwave absorption of reduced graphene oxide/zinc ferrite hybrid nanocomposite, Mater. Lett. 215 (2018) 229–232.
[33] G. Zhang, R. Shu, Y. Xie, H. Xia, Y. Gan, J. Shi, J. He, Cubic $MnFe_2O_4$ particles decorated reduced graphene oxide with superior microwave absorption properties, Mater. Lett. 231 (2018) 209–212.
[34] J. Peng, Z. Peng, Z. Zhu, R. Augustineb, M. Mahmoud, H. Tang, M. Rao, Y. Zhang, G. Li, T. Jiang, Achieving ultra-high electromagnetic wave absorption by anchoring $Co_{0.33}Ni_{0.33}Mn_{0.33}Fe_2O_4$ nanoparticles on graphene sheets using microwave-assisted polyol method, Ceram. Int. 44 (2018) 21015–21026.
[35] W. Shen, B. Ren, K. Cai, Y. Song, W. Wang, Synthesis of nonstoichiometric $Co_{0.8}Fe_{2.2}O_4$/reduced graphene oxide (rGO) nanocomposites and their excellent electromagnetic wave absorption property, J. Alloy. Compd. 774 (2019) 997–1008.
[36] T. Zhu, S. Chang, Y. Song, M. Lahoubic, W. Wang, PVP-encapsulated $CoFe_2O_4$/rGO composites with controllable electromagnetic wave absorption performance, Chem. Eng. J. 373 (2019) 755–766.
[37] M. Gao, Y. Zhao, S. Wang, Y. Xu, C. Feng, D. Shi, Q. Jiao, Preparation of pod-like 3D $Ni_{0.33}Co_{0.67}Fe_2O_4$@rGO composites and their microwave absorbing properties, Ceram. Int. 45 (2019) 7188–7195.
[38] F. Wu, A. Xie, M. Sun, Y. Wang, M. Wang, Reduced graphene oxide (RGO) modified spongelike polypyrrole (PPy) aerogel for superior electromagnetic absorption, J. Mater. Chem. A 3 (2015) 14358–14369.
[39] P. Xie, H. Li, B. He, F. Dang, J. Lin, R. Fan, C. Hou, H. Liu, J. Zhang, Y. Ma, Z. Guo, Bio-gel derived nickel/carbon nanocomposites with enhanced microwave absorption, J. Mater. Chem. C 6 (2018) 8812–8822.
[40] C. Zhou, C. Wu, H. Lv, M. Yan, Porous $Co_9S_8$ nanotubes with the percolation effect for lightweight and highly efficient electromagnetic wave absorption, J. Mater. Chem. C 7 (2019) 1696–1704.
[41] C. Chen, S. Bao, B. Zhang, Y. Zhou, S. Li, Development of sulfide-doped Graphene/$Fe_3O_4$ absorber with wide band electromagnetic absorption performance, J. Alloy. Compd. 770 (2019) 90–97.
[42] X. Gao, Y. Wang, Q. Wang, X. Wu, W. Zhang, C. Luo, Facile synthesis of hollow cube-like $ZnSnO_3$ wrapped by nitrogen-doped graphene: as a high-performance and enhanced synergistic microwave absorber, J. Magn. Magn. Mater. 486 (2019) 165251.
[43] J. Feng, Y. Zong, Y. Sun, Y. Zhang, X. Yang, G. Long, Y. Wang, X. Li, X. Zheng, Optimization of porous $FeNi_3$/N-GN composites with superior microwave absorption performance, Chem. Eng. J. 345 (2018) 441–451.
[44] X. Wang, T. Ma, J. Shu, M. Cao, Confinedly tailoring $Fe_3O_4$ clusters-NG to tune electromagnetic parameters and microwave absorption with broadened bandwidth, Chem. Eng. J. 332 (2018) 321–330.
[45] Z. Li, X. Li, Y. Zong, G. Tan, Y. Sun, Y. Lan, M. He, Z. Ren, X. Zheng, Solvothermal synthesis of nitrogen-doped graphene decorated by superparamagnetic $Fe_3O_4$ nanoparticles and their applications as enhanced synergistic microwave absorbers, Carbon 115 (2017) 493–502.
[46] J. Feng, F. Pu, Z. Li, X. Li, X. Hu, J. Bai, Interfacial interactions and synergistic effect of CoNi nanocrystals and nitrogen-doped graphene in a composite microwave absorber, Carbon 104 (2016) 214–225.
[47] R. Shu, J. Zhang, Y. Wu, Z. Wan, M. Zheng, Facile design of nitrogen-doped reduced graphene oxide/zinc ferrite hybrid nanocomposites with excellent microwave absorption in the X-band, Mater. Lett. 255 (2019) 126549.
[48] R. Shu, G. Zhang, X. Wang, X. Gao, M. Wang, Y. Gan, J. Shi, J. He, Fabrication of 3D net-like MWCNTs/$ZnFe_2O_4$ hybrid composites as high-performance electromagnetic wave absorbers, Chem. Eng. J. 337 (2018) 242–255.
[49] R. Shu, G. Zhang, J. Zhang, X. Wang, M. Wang, Y. Gan, J. Shi, J. He, Fabrication of reduced graphene oxide/multi-walled carbon nanotubes/zinc ferrite hybrid composites as high-performance microwave absorbers, J. Alloy. Compd. 736 (2018) 1–11.
[50] D. Chen, X. Tang, J. Wu, W. Zhang, Q. Liu, Y. Jiang, Effect of grain size on the magnetic properties of superparamagnetic $Ni_{0.5}Zn_{0.5}Fe_2O_4$ nanoparticles by co-precipitation process, J. Magn. Magn. Mater. 323 (2011) 1717–1721.
[51] R. Shu, W. Li, X. Zhou, D. Tian, G. Zhang, Y. Gan, J. Shi, J. He, Facile preparation and microwave absorption properties of RGO/MWCNTs/$ZnFe_2O_4$ hybrid nanocomposites, J. Alloy. Compd. 743 (2018) 163–174.
[52] Q. Liu, X. Liu, H. Feng, H. Shui, R. Yu, Metal organic framework-derived Fe/carbon porous composite with low Fe content for lightweight and highly efficient electromagnetic wave absorber, Chem. Eng. J. 314 (2017) 320–327.
[53] Y. Yin, X. Liu, X. Wei, Y. Li, X. Nie, R. Yu, J. Shui, Magnetically aligned Co-C/MWCNTs composite derived from MWCNT-interconnected zeolitic imidazolate frameworks for a lightweight and highly efficient electromagnetic wave absorber, ACS Appl. Mater. Interfaces 9 (2017) 30850–30861.
[54] B. Quan, X. Liang, G. Xu, Y. Cheng, Y. Zhang, W. Liu, G. Ji, Y. Du, A permittivity regulating strategy to achieve high-performance electromagnetic wave absorbers with compatibility of impedance matching and energy conservation, New J. Chem. 41 (2017) 1259–1266.
[55] L. Yin, T. Chen, S. Liu, Y. Gao, B. Wu, Y. Wei, G. Li, X. Jian, X. Zhang, Preparation and microwave-absorbing property of $BaFe_{12}O_{19}$ nanoparticles and $BaFe_{12}O_{19}$/$Fe_3C$/CNTs composites, RSC Adv. 5 (2015) 91665–91669.
[56] J. Zhou, X. Shu, Z. Wang, Y. Liu, Y. Wang, C. Zhou, L. Kong, Hydrothermal synthesis of polyhedral FeCo alloys with enhanced electromagnetic absorption performances, J. Alloy. Compd. 794 (2019) 68–75.
[57] B. Zhao, B. Fan, G. Shao, W. Zhao, R. Zhang, Facile synthesis of novel heterostructure based on $SnO_2$ nanorods grown on submicron Ni walnut with tunable electromagnetic wave absorption capabilities, ACS Appl. Mater. Interfaces 7 (2015) 18815–18823.
[58] B. Zhao, G. Shao, B. Fan, W. Zhao, R. Zhang, Facile synthesis and enhanced microwave absorption properties of novel hierarchical heterostructures based on a Ni microsphere–CuO nano-rice core–shell composite, PCCP 17 (2015) 6044–6052.
[59] M. Cao, X. Wang, M. Zhang, J. Shu, W. Cao, H. Yang, X. Fang, J. Yuan, Electromagnetic response and energy conversion for functions and devices in low-dimensional materials, Adv. Funct. Mater. 1807398 (2019).
[60] P. Wang, J. Zhang, G. Wang, B. Duan, D. He, T. Wang, F. Li, Synthesis and characterization of $MoS_2$/Fe@$Fe_3O_4$ nanocomposites exhibiting enhanced microwave absorption performance at normal and oblique incidences, J. Mater. Sci. Technol. 35 (2019) 1931–1939.
[61] T. Wang, L. Qiao, R. Han, Z. Zhang, The origin of reflection loss peaks in the double-layer electromagnetic wave absorber, J. Magn. Magn. Mater. 324 (2012) 3209–3212.
[62] B. Wang, J. Wei, L. Qiao, T. Wang, F. Li, Influence of the interface reflections on the microwave reflection loss for carbonyl iron/paraffin composite backed by a perfect conduction plate, J. Magn. Magn. Mater. 324 (2012) 761–765.
[63] Y. Wang, X. Gao, X. Wu, W. Zhang, Q. Wang, C. Luo, Hierarchical $ZnFe_2O_4$@RGO@CuS composite: strong absorption and wide-frequency absorption properties, Ceram. Int. 44 (2018) 9816–9822.
[64] W. Liu, Q. Shao, G. Ji, X. Liang, Y. Cheng, B. Quan, Y. Du, Metal–organic-frameworks derived porous carbon-wrapped Ni composites with optimized impedance matching as superior lightweight electromagnetic wave absorber, Chem. Eng. J. 313 (2017) 734–744.
[65] D. Li, B. Zhang, W. Liu, X. Liang, G. Ji, Tailoring the input impedance of FeCo/C composites with efficient broadband absorption, Dalton Trans. 46 (2017) 14926–14933.
[66] W. Song, M. Cao, Z. Hou, X. Fang, X. Shi, J. Yuan, High dielectric loss and its monotonic dependence of conducting-dominated multiwalled carbon nanotubes/silica nanocomposite on temperature ranging from 373 to 873 K in X-band, Appl. Phys. Lett. 94 (2009) 233110.
[67] M. Cao, W. Song, Z. Hou, B. Wen, J. Yuan, The effects of temperature and frequency on the dielectric properties, electromagnetic interference shielding and microwave-absorption of short carbon fiber/silica composites, Carbon 48 (2010) 788–796.
[68] M. Cao, X. Wang, W. Cao, X. Fang, B. Wen, J. Yuan, Thermally driven transport and relaxation switching self-powered electromagnetic energy conversion, Small 14 (2018) 1800987.